

## Localized defect modes in graphene

Alexander V. Savin<sup>1,2</sup> and Yuri S. Kivshar<sup>1</sup><sup>1</sup>*Nonlinear Physics Center, Research School of Physics and Engineering, Australian National University, Canberra ACT 0200, Australia*<sup>2</sup>*Semenov Institute of Chemical Physics, Russian Academy of Sciences, Moscow 119991, Russia*

(Received 15 May 2013; revised manuscript received 18 July 2013; published 11 September 2013)

We study the properties of localized vibrational modes associated with structural defects in a sheet of graphene. For the examples of the Stone-Wales defects, one- and two-atom vacancies, many-atom linear vacancies, and adatoms in a honeycomb lattice, we demonstrate that the local defect modes are characterized by stable oscillations with the frequencies lying outside the linear frequency bands of an ideal graphene. In the frequency spectral density of thermal oscillations, such localized defect modes lead to the additional peaks from the right side of the frequency band of the ideal sheet of graphene, which indicate the presence of defects in the graphene flakes.

DOI: [10.1103/PhysRevB.88.125417](https://doi.org/10.1103/PhysRevB.88.125417)

PACS number(s): 63.20.-e, 63.22.Rc

### I. INTRODUCTION

Over the past 20 years, nanotechnology has made an impressive impact on the development of many fields of physics, chemistry, medicine, and nanoscale engineering. The discovery of carbon nanotubes and graphene as novel materials for nanotechnology<sup>1,2</sup> has attracted many efforts in the study of their unusual properties. In particular, many properties of graphene originate from the fact that it has a two-dimensional structure that brings many novel features that are studied both theoretically and experimentally.<sup>3,4</sup>

Usually, depending on the type of growth and fabrication procedure employed, the graphene surface has structural defects which may substantially change its mechanical, electronic, and transport properties. Structural defects may also change both electronic and phononic spectra of the graphene. Moreover, defects create additional sources of scattering for phonons and electrons, so they may substantially alter the transport properties of graphene structures.

By adding defects to an ideal graphene, we may change its properties, and this is the main concept of nanoengineering of defect structures on graphene. In particular, local defects may change the absorbing properties of graphene,<sup>5</sup> whereas extended defects allow the use of graphene as a membrane for gas separation,<sup>6</sup> and arrays of defects may change the conducting properties of graphene structures.<sup>7,8</sup>

We may divide various localized defects in graphene into two classes: point defects (such as the Stone-Wales defect, vacancies, and adatoms) and one-dimensional dislocationlike defects.<sup>9</sup> Point defects in graphene act as scattering centers for electron and phonon waves.<sup>10-12</sup> Linear defects are responsible for plastic deformations of graphene nanoribbons.

Linear defects are known to be responsible for plastic deformations of graphene nanotubes,<sup>13</sup> so we may naturally expect that defects will be important for plastic deformation in graphene nanoribbons. However, as a matter of fact, there exists very limited knowledge on the oscillatory dynamics of the defects in graphene, whereas the structure of graphene with defects is studied more thoroughly,<sup>7,9</sup> as well as the role of defect in the electron conductivity, which is considered in many publications.<sup>14-17</sup> In this paper, we provide a systematic study of the linear oscillatory dynamics of defects in graphene and thermal conductivity of graphene with defects; we also

present a study of nonlinear dynamics of isolated defects in graphene, revealing their interesting properties.

Extended linear arrays of defects may substantially modify the thermal properties of graphene nanoribbons. A linear defect running along the nanoribbon behaves as an effective third edge of the structure, giving rise to new conduction pathways that could be used in nanoscale circuitry as a quantum wire.<sup>14</sup> The creation of a linear array of defect in the center of zigzag graphene may modify its magnetic properties, transforming antiferromagnetic states to ferromagnetic states,<sup>18,19</sup> as well as electron properties.<sup>15,20,21</sup> Defect lines may also change other properties of graphene flakes and nanoribbons related to their phonon transport, e.g., arrays of defects may lower thermal conductivity.<sup>22,23</sup> If the localized oscillations are excited on defects placed in close proximity, they may overlap, creating an effective waveguide supporting the frequency band of phonon conductivity.

In this paper, we study the oscillatory phonon modes localized at the point defects in graphene. To the best of our knowledge, this problem was never analyzed in detail. In particular, we apply the molecular dynamics numerical simulations and demonstrate that each type of structural defect supports a number of localized modes with the frequencies located outside the frequency bands of the ideal graphene lattice. We also analyze nonlinear properties of these localized modes and demonstrate that their frequencies decrease when the input power grows. Such isolated frequency peaks observed in the oscillatory spectrum of the graphene flake may serve as fingerprints of localized modes excited at the point defects. In addition, we study the properties of an array of defects and demonstrate that such an array creates an efficient waveguide for high-frequency phonons.

The paper is organized as follows. In Sec. II, we describe our microscopic model and introduce the interaction potentials. Section III summarizes the types of the local defects in graphene analyzed in the paper. Sections IV and V are devoted to the analysis of the properties of in-plane and out-of-plane defect modes. In Secs. VI and VII, we analyze how the defect modes are manifested in the dynamics and thermalized relaxation of graphene structures. In Sec. VIII, we analyze an array of defects placed in the middle of a graphene nanoribbon and demonstrate that it can operate as an efficient

phonon waveguide, enhancing the thermal conductivity of the nanoribbon. Section IX concludes the paper.

## II. MODEL

To model numerically the oscillations of the graphene sheet with local defects, we consider a rectangular graphene lattice of a finite extent (a graphene flake) with the size  $10.8 \times 10.6 \text{ nm}^2$  composed of  $N = 4400$  carbon atoms. We place a defect at the center of this graphene flake and introduce a periodic boundary condition to avoid the interaction with the boundaries.

To describe graphene oscillations, we write the system Hamiltonian in the form

$$H = \sum_{n=1}^N \left[ \frac{1}{2} M (\dot{\mathbf{u}}_n, \dot{\mathbf{u}}_n) + P_n \right], \quad (1)$$

where  $M = 12m_p$  is the mass of the carbon atom ( $m_p$  is the proton mass) and  $\mathbf{u}_n = [x_n(t), y_n(t), z_n(t)]$  is the radius vector of the carbon atom with the index  $n$  at the moment  $t$ . The term  $P_n$  describes the interaction of the atom with the index  $n$  and its neighboring atoms. The potential energy depends on variations in bond length, bond angles, and dihedral angles between the planes formed by three neighboring carbon atoms and can be written in the form

$$P = \sum_{\Omega_1} U_1 + \sum_{\Omega_2} U_2 + \sum_{\Omega_3} U_3 + \sum_{\Omega_4} U_4 + \sum_{\Omega_5} U_5, \quad (2)$$

where  $\Omega_i$ , with  $i = 1, 2, 3, 4, 5$ , are the sets of configurations including up to nearest-neighbor interactions. Owing to a large redundancy, the sets only need to contain configurations of the atoms shown in Fig. 1, including their rotated and mirrored versions.

The potential  $U_1(\mathbf{u}_\alpha, \mathbf{u}_\beta)$  describes the deformation energy due to a direct interaction between pairs of atoms with the indexes  $\alpha$  and  $\beta$ , as shown in Fig. 1(a). The potential  $U_2(\mathbf{u}_\alpha, \mathbf{u}_\beta, \mathbf{u}_\gamma)$  describes the deformation energy of the angle between the valent bonds  $\mathbf{u}_\alpha \mathbf{u}_\beta$  and  $\mathbf{u}_\beta \mathbf{u}_\gamma$ ; see Fig. 1(b). Potentials  $U_i(\mathbf{u}_\alpha, \mathbf{u}_\beta, \mathbf{u}_\gamma, \mathbf{u}_\delta)$ ,  $i = 3, 4, 5$ , describe the deformation energy associated with a change of the effective angle between the planes  $\mathbf{u}_\alpha, \mathbf{u}_\beta, \mathbf{u}_\gamma$  and  $\mathbf{u}_\beta, \mathbf{u}_\gamma, \mathbf{u}_\delta$ , as shown in Figs. 1(c)–1(e).

We use the potentials employed in the modeling of the dynamics of large polymer macromolecules<sup>24–28</sup> for the valent bond coupling,

$$U_1(\mathbf{u}_1, \mathbf{u}_2) = \epsilon_1 \{ \exp[-\alpha_0(\rho - \rho_0)] - 1 \}^2, \quad (3)$$

$$\rho = |\mathbf{u}_2 - \mathbf{u}_1|,$$

where  $\epsilon_1 = 4.9632 \text{ eV}$  is the energy of the valent bond and  $\rho_0 = 1.418 \text{ \AA}$  is the equilibrium length of the bond; the

potential of the valent angle is

$$U_2(\mathbf{u}_1, \mathbf{u}_2, \mathbf{u}_3) = \epsilon_2 (\cos \varphi - \cos \varphi_0)^2, \quad (4)$$

$$\cos \varphi = (\mathbf{u}_3 - \mathbf{u}_2, \mathbf{u}_1 - \mathbf{u}_2) / (|\mathbf{u}_3 - \mathbf{u}_2| \cdot |\mathbf{u}_2 - \mathbf{u}_1|),$$

so that the equilibrium value of the angle is defined as  $\cos \varphi_0 = \cos(2\pi/3) = -1/2$ ; the potential of the torsion angle is

$$U_i(\mathbf{u}_1, \mathbf{u}_2, \mathbf{u}_3, \mathbf{u}_4) = \epsilon_i (1 - z_i \cos \phi),$$

$$\cos \phi = (\mathbf{v}_1, \mathbf{v}_2) / (|\mathbf{v}_1| \cdot |\mathbf{v}_2|), \quad (5)$$

$$\mathbf{v}_1 = (\mathbf{u}_2 - \mathbf{u}_1) \times (\mathbf{u}_3 - \mathbf{u}_2),$$

$$\mathbf{v}_2 = (\mathbf{u}_3 - \mathbf{u}_2) \times (\mathbf{u}_3 - \mathbf{u}_4),$$

where the sign  $z_i = 1$  for the indices  $i = 3, 4$  (equilibrium value of the torsional angle  $\phi_0 = 0$ ) and  $z_i = -1$  for the index  $i = 5$  ( $\phi_0 = \pi$ ).

The specific values of the parameters are  $\alpha_0 = 1.7889 \text{ \AA}^{-1}$ ,  $\epsilon_2 = 1.3143 \text{ eV}$ , and  $\epsilon_3 = 0.499 \text{ eV}$ , and they are found from the frequency spectrum of small-amplitude oscillations of a sheet of graphite.<sup>29</sup> According to the results of Ref. 30, the energy  $\epsilon_4$  is close to the energy  $\epsilon_3$ , whereas  $\epsilon_5 \ll \epsilon_4$  ( $|\epsilon_5/\epsilon_4| < 1/20$ ). Therefore, in what follows, we use the values  $\epsilon_4 = \epsilon_3 = 0.499 \text{ eV}$  and assume  $\epsilon_5 = 0$ ; the latter means that we omit the last term in the sum (2).

More detailed discussion and motivation of our choice of the interaction potentials (2)–(4) can be found in Ref. 31. Such potentials have been employed for the modeling of thermal conductivity of carbon nanotubes,<sup>32,33</sup> graphene nanoribbons,<sup>31</sup> and also in the analysis of their oscillatory modes.<sup>34–36</sup>

We notice that the graphene dynamics is modeled in many papers by the so-called Brenner potential,<sup>37</sup> instead of the potentials  $U_1, \dots, U_4$  introduced above. However, as we demonstrated in our earlier studies, this potential does not describe well the high-frequency part of the oscillatory spectrum. For example, the Brenner potential does not correctly predict the degeneracy of the frequency spectrum, so that the equilibrium shape of the  $C_{60}$  molecule slightly deviates from the icosahedra shape.<sup>38</sup> Therefore, we do not employ this potential in our work.

## III. TYPES OF LOCALIZED DEFECTS IN GRAPHENE

First, we introduce a model of graphene with defects. In order to model the defect dynamics in an infinite graphene sheet, we consider a graphene of a finite extent with periodic boundary conditions. To avoid the possible influence of the edge effects, we take an almost rectangular honeycomb lattice with the size  $10.6 \times 10.5 \text{ nm}^2$  consisting of  $N = 4400$  carbon atoms, as shown in Figs. 2(a) and 3. It is important to mention that the plots in the Supplemental Material<sup>39</sup> show only the central area, which is a small fraction of the simulation results,

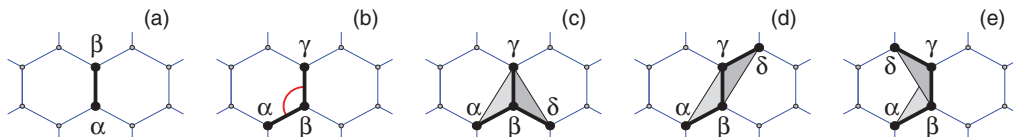


FIG. 1. (Color online) Configurations containing up to the  $i$ th nearest-neighbor interactions for  $i =$  (a) 1, (b) 2, (c) 3, (d) 4, and (e) 5.

in fact, about 5% of the area of the graphene flake simulated numerically. Indeed, the shown fragment is  $3.3 \times 3.3 \text{ nm}^2$  and consists of 224 atoms only. The defect is placed at the center and its oscillations move  $N_d$  atoms. For all defects studied in our work, we have  $N_d < 147$ , and therefore the condition  $N_d \ll N$  is always satisfied.

Depending on the type of defect we create, we add or remove some carbon atoms at its center by cutting the corresponding bonds. In this way, we define the atomic

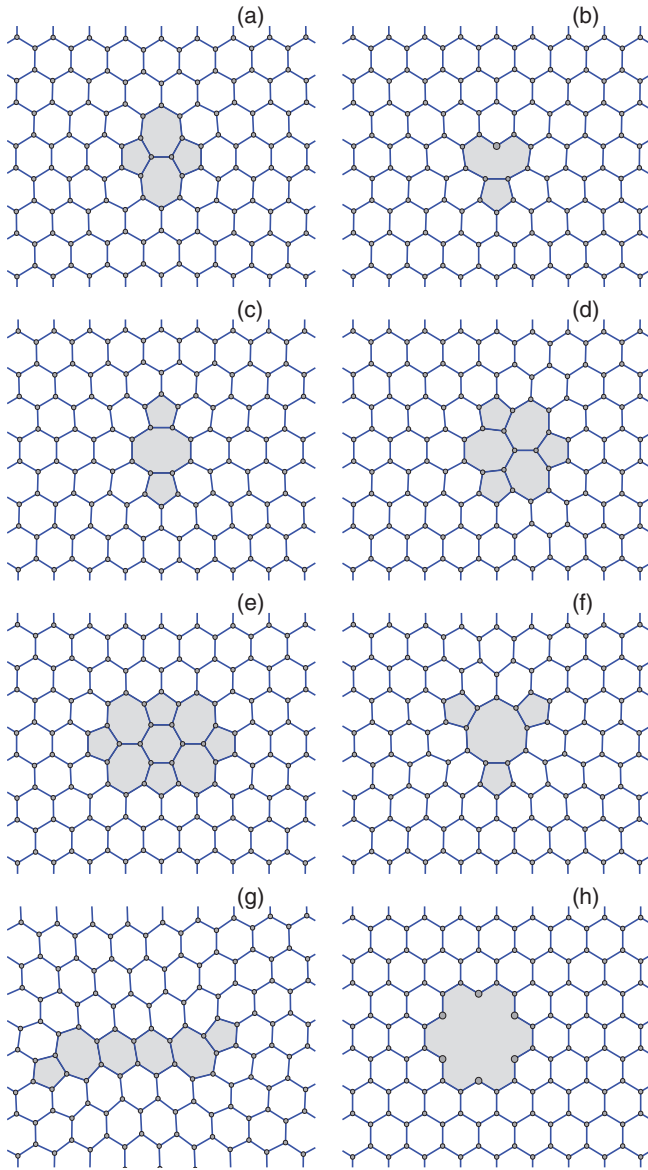


FIG. 2. (Color online) Localized defects which do not change the flat surface of the graphene layer: (a) Stone-Wales defect SW(55-77), (b) single vacancy  $V_1(5-9)$ , (c) double vacancy  $V_2(5-8-5)$ , (d) double vacancy  $V_2(555-777)$ , (e) double vacancy  $V_2(5555-6-7777)$ , (f) quadruple vacancy  $V_4(555-9)$ , (g) vacancy  $V_8(5-7-66-7-5)$  is an extended linear defect obtained by removing a zigzaglike array of eight carbon atoms, (h) vacancy  $V_6$  is a defect created by removing six carbon atoms with the formation of a hexagonal hole. The gray color is employed to show a change of the lattice structure introduced by the presence of a defect.

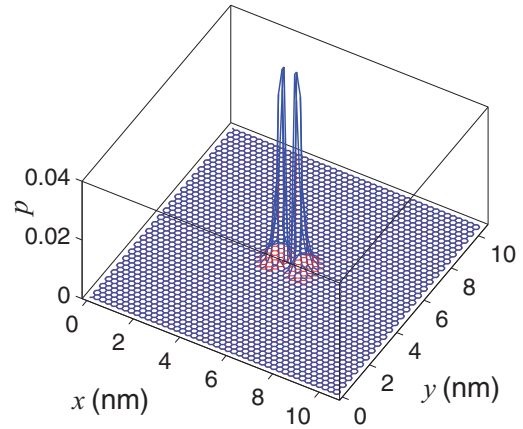


FIG. 3. (Color online) Energy of in-plane oscillations for the Stone-Wales defect SW(55-77) with the frequency  $\omega_d = 1613.2 \text{ cm}^{-1}$  and the participation number  $N_d = 26.31$ .

configuration  $\{\mathbf{u}_n\}_{n=1}^N$  that will relax to the structure with a specific type of defect. To find the ground state of the graphene layer with defects, we should find the energy minimum for the interaction energy,

$$\sum_{n=1}^N P_n \rightarrow \min : \{\mathbf{u}_n\}_{n=1}^N. \quad (6)$$

Problem (6) is solved numerically by means of the conjugate gradient method. If  $\{\mathbf{u}_n^0\}_{n=1}^N$  is the ground state of this rectangular flake of graphene, then, for small-amplitude oscillations, we can write  $\mathbf{u}_n(t) = \mathbf{u}_n^0 + \mathbf{v}_n(t)$ , where  $|\mathbf{v}_n| \ll \rho_0$ . Then, the equations of motion corresponding to the Hamiltonian (1) can be written as a system of  $3N$  linear equations for  $3N$  variables,

$$-M\ddot{\mathbf{v}}_n = \frac{\partial H}{\partial \mathbf{u}_n} = \sum_{j=1}^N B_{jn} \mathbf{v}_j, \quad B_{jn} = \left. \frac{\partial^2 H}{\partial \mathbf{u}_n \partial \mathbf{u}_j} \right|_{\{\mathbf{u}_k^0\}_{k=1}^N}. \quad (7)$$

To find all linear modes of the graphene sheet, we need to find numerically all  $3N \times 3N$  eigenvalues and corresponding eigenvectors of the real symmetric matrix  $\mathbf{B} = (B_{jn})_{j,n=1}^N$ . If we define  $\lambda$  and  $\mathbf{e} = \{\mathbf{v}_n^0\}_{n=1}^N$  as the eigenvalue and normalized eigenvector, namely,  $\mathbf{B}\mathbf{e} = \lambda\mathbf{e}$  and  $(\mathbf{e}, \mathbf{e}) = \sum_{n=1}^N (\mathbf{v}_n^0, \mathbf{v}_n^0) = 1$ , then the solution of Eq. (7) will have the form  $\mathbf{v}_n(t) = A\mathbf{v}_n^0 \exp(i\omega t)$ , where  $\omega = \sqrt{\lambda/M}$  is the mode frequency and  $A$  is the mode amplitude.

We characterize the degree of spatial localization of any of the oscillatory eigenmodes by the parameter of localization (inverse participation number),  $d = \sum_{n=1}^N (\mathbf{v}_n^0, \mathbf{v}_n^0)^2$ . For the modes which are not localized in space,  $d \approx 1/N$ , and for the mode localized on a single atom,  $d = 1$ . The inverse value  $N_d = 1/d$  (participation number) characterizes the number of atoms which are involved in this oscillatory mode. It will be clear from the results presented below that the participation number of the involved defect modes is  $2.6 < N_d < 147$ , and the condition  $N_d \ll N = 4400$  always holds. Therefore, the size of the simulated graphene flake is large enough to neglect any edge effects.

For an ideal flake of graphene, all eigenmodes are delocalized and, for the periodic boundary conditions, they

are distributed homogeneously on the rectangular surface. All such oscillatory modes can be divided into two classes: (i) in-plane modes, when the atoms oscillate along the flat surface of the graphene sheet, and (ii) out-of-plane modes, when the atoms oscillate perpendicular to the surface of the graphene sheet. The frequencies of the former modes are located in the domain  $0 \leq \omega \leq 1600 \text{ cm}^{-1}$ , whereas the frequencies of the latter modes correspond to a narrow spectral range,  $0 \leq \omega \leq 900 \text{ cm}^{-1}$ .

Different types of defect in a hexagonal lattice of graphene have been described in detail in a recent review paper.<sup>9</sup> The existence of many such defects has been confirmed experimentally. We use the classification and definitions adopted in that review paper and analyze the dynamic properties of all major types of defects.

We notice that the effective potentials  $U_1, \dots, U_4$  used here allow one to describe all types of defects, and our results for the defect configuration coincide with the earlier results.<sup>9</sup>

In what follows, first we study the in-plane localized defects shown in Fig. 2 which do not bend the surface of the graphene sheet (Sec. IV), but then consider the case of out-of-plane defects (Sec. V).

The oscillatory dynamics of all localized modes is shown in movies in the Supplemental Material.<sup>39</sup> There, the name of each “gif” file corresponds to the type and frequency of the corresponding defect mode (for example, file I\_2\_1605.gif corresponds to defect mode  $I_2$  with frequency  $\omega_d = 1604.8 \text{ cm}^{-1}$ ).

#### IV. OSCILLATIONS OF IN-PLANE DEFECTS

To create the Stone-Wales defect SW(55-77), we should rotate one valent bond by 90 degrees. Then, four old neighboring valent bonds break, creating four new bonds. As a result, we create two pentagons and two heptagons (55-77) instead of four hexagons of the perfect honeycomb lattice, as shown in Fig. 2(a). In the ground state, this defect has the energy  $E_d = 2.06 \text{ eV}$  and is stable. Although the defect’s energy is higher than that of the ground state by the value  $E_d$ , the reverse change of the bonds requires that the energy barrier of  $\Delta E = 9 \text{ eV}$  be overtaken.<sup>9</sup>

Our analysis of the localized modes of the lattice with the defect shows that the Stone-Wales defect supports four in-plane localized modes with the frequencies  $\omega_d = 1613.2, 1614.1, 1615.6, \text{ and } 1616.3 \text{ cm}^{-1}$  (and the participation numbers  $N_d = 26.31, 27.06, 25.65, 26.14$ ) and also four out-of-plane localized modes with the frequencies  $\omega_d = 904.7, 907.5, 909.4, \text{ and } 935.1 \text{ cm}^{-1}$  ( $N_d = 44.74, 21.81, 37.24, 7.90$ ). The characteristic profile of the oscillatory energy of this defect mode is shown in Fig. 3, where we observe that the energy is localized entirely in the region of the defect, so the used periodic boundary conditions do not have any influence on the mode’s frequency and shape. See also the following animation files in the Supplemental Material:<sup>39</sup> SW(5577)\_905.gif through SW(5577)\_1616.gif.

In order to create a single vacancy  $V_1(5-9)$  in the graphene lattice, we remove just one carbon atom breaking three valent bonds. The remaining lattice relaxes with two neighboring atoms linked by a new valent bond and, instead of three hexagons, the structure (5-9) is formed with one pentagon and one nonagon; see Fig. 2(b). In this defect structure, one

carbon atom has only two valent bonds. In order to keep the interaction potentials of those bonds unchanged in our calculations, we assume that this atom is coupled to a hydrogen atom and has mass  $M = 13m_p$ . Then the energy of the defect  $V_1(5-9)$  is found to be  $E_d = 2.26 \text{ eV}$ . This defect supports three in-plane localized eigenmodes with the frequencies  $\omega_d = 1600.6, 1601.3, \text{ and } 1606.3 \text{ cm}^{-1}$  ( $N_d = 146.99, 79.41, 14.58$ ) and two out-of-plane lightly localized modes with the frequencies  $\omega_d = 1227.0 \text{ and } 1791.0 \text{ cm}^{-1}$  ( $N_d = 5.03, 2.65$ ). See also the following animation files in the Supplemental Material:<sup>39</sup> V\_1\_1227.gif through V\_1\_1791.gif.

The double-vacancy defect  $V_2(5-8-5)$  shown in Fig. 2(c) can be created by removing two neighboring carbon atoms, breaking four valent bonds. After this procedure, the remaining four neighboring carbon atoms create two new valent bonds and, in the lattice structure, four hexagons are replaced by two pentagons and one octagon. The energy of the double-vacancy defect  $V_2(5-8-5)$  is found to be  $E_d = 3.44 \text{ eV}$ . This defect supports four in-plane eigenmodes of localized oscillations with the frequencies  $\omega_d = 1605.9, 1606.0, 1619.2, \text{ and } 1619.3 \text{ cm}^{-1}$  ( $N_d = 65.91, 66.16, 15.21, 15.32$ ) and four out-of-plane localized modes with the frequencies  $\omega_d = 902.6, 905.0, 986.4, \text{ and } 1015.0 \text{ cm}^{-1}$  ( $N_d = 64.16, 57.77, 6.18, 7.27$ ). See also the following animation files in the Supplemental Material:<sup>39</sup> V\_2(585)\_903.gif through V\_2(585)\_1619.gif.

In order to create the double-vacancy defect  $V_2(555-777)$ , we should start from the defect  $V_2(5-8-5)$  and rotate one of the bonds of its octagon by 90 degrees. Then four old bonds break and four new bonds appear. In the graphene lattice, instead of seven hexagons, we obtain three pentagons and three heptagons (555-777), as shown in Fig. 2(d). This defect is characterized by the energy  $E_d = 2.91 \text{ eV}$ . Our analysis of the eigenmodes localized on this defect demonstrates that it has no in-plane localized modes at all, but it supports four out-of-plane modes with the frequencies  $\omega_d = 909.1, 916.0, 916.0, \text{ and } 916.6 \text{ cm}^{-1}$  ( $N_d = 46.22, 15.87, 15.87, 11.30$ ). See also the following animation files in the Supplemental Material:<sup>39</sup> V\_2(555777)\_909.gif through V\_2(555777)\_917.gif.

The double-vacancy defect  $V_2(5555-6-7777)$  is formed from the defect  $V_2(555-777)$  by another bond rotation. In the honeycomb lattice, instead of ten perfect hexagons, we have four pentagons, one hexagon, and four heptagons, as shown in Fig. 2(e). The energy of this double-vacancy defect is  $E_d = 2.96 \text{ eV}$ . This defect supports seven localized in-plane eigenmodes with the frequencies  $\omega_d = 1605.5, 1605.6, 1607.3, 1607.4, 1666.4, 1773.7, \text{ and } 2009.4 \text{ cm}^{-1}$  (and the participation numbers  $N_d = 25.84, 25.50, 25.99, 23.65, 5.86, 4.57, 3.05$ ) and four out-of-plane localized modes with the frequencies  $\omega_d = 905.7, 907.2, 916.4, \text{ and } 918.4 \text{ cm}^{-1}$  ( $N_d = 46.72, 54.22, 15.07, 14.52$ ). See also the following animation files in the Supplemental Material:<sup>39</sup> V\_2(555567777)\_906.gif through V\_2(555567777)\_2009.gif.

The largest hole appears when we remove four neighboring carbon atoms from the graphene lattice with Y-shape valent bonds. After that, six carbon atoms coupled to the removed atom get involved into new valent bonds, thus creating quadruple vacancy defect  $V_4(555-9)$ . In this defect, instead of six hexagons, we have three heptagons and one large nonagon, as shown in Fig. 2(f). The energy of this defect is

$E_d = 5.37$  eV. This defect supports three in-plane eigenmodes with the frequencies  $\omega_d = 1601.9, 1602.4,$  and  $1602.4$   $\text{cm}^{-1}$  (participation numbers  $N_d = 59.02, 40.46, 40.21$ ) and also four out-of-plane modes with the frequencies  $\omega_d = 902.3, 908.9, 976.6,$  and  $997.3$   $\text{cm}^{-1}$  ( $N_d = 52.27, 11.01, 7.23, 6.51$ ).

For comparison, next we consider an extended defect in the form of the vacancy  $V_8(5-7-66-7-5)$ , which appears after removing a zigzag chain of an array of eight carbon atoms, shown in Fig. 2(g). In the honeycomb lattice, instead of ten perfect hexagons, we create two pentagons, two hexagons, and two heptagons; the defect energy is  $E_d = 11.92$  eV. This extended defect supports seven in-plane localized modes with the frequencies  $\omega_d = 1604.2, 1606.8, 1607.2, 1613.4, 1624.3, 1627.3,$  and  $1653.2$   $\text{cm}^{-1}$  ( $N_d = 57.72, 19.39, 18.03, 11.53, 10.67, 11.49, 4.36$ ) and also four out-of-plane localized modes with the frequencies  $\omega_d = 909.3, 910.5, 927.2,$  and  $1091.0$   $\text{cm}^{-1}$  corresponding to  $N_d = 21.35, 21.53, 6.25,$  and  $2.69$ . See also the following animation files in the Supplemental Material:<sup>39</sup> V\_8\_909.gif through V\_8\_1654.gif.

If we remove one hexagon from the honeycomb lattice, we create a vacancy  $V_6$  that cannot be “healed” by the lattice transformations. This vacancy has the form of a perfect hexagon hole with the diameter of  $0.57$  nm, with almost unchanged old valent bonds; see Fig. 2(h). Our analysis demonstrates that such holes do not support any localized modes.

## V. OSCILLATIONS OF OUT-OF-PLANE DEFECTS

Unlike vacancies, adding extra atoms to the graphene sheet leads to a deformation of the planar structure of the lattice. In the place where we have more atoms, the graphene sheet is no longer flat and becomes either concave or convex, transforming into one of the two equivalent nonplanar states.

When two migrating adatoms meet each other and form a dimer, they can be incorporated into the graphene lattice, creating the so-called inverse Stone-Wales defect  $I_2(7557)$ . In such a state, instead of three hexagons, we have two pentagons and two heptagons, as shown in Fig. 4(a). The surface of the sheet becomes deformed, bending into either side.

Our analysis shows that such a defect supports eight localized modes for which atoms move along the curved surface. The mode eigenfrequencies are  $\omega_d = 1604.8, 1613.1, 1624.2, 1641.3, 1644.2, 1650.7, 1723.5,$  and  $1749.4$   $\text{cm}^{-1}$  (with the participation numbers  $N_d = 73.63, 5.93, 19.82, 6.73, 8.64, 12.37, 3.14, 2.85$ ). This defect also supports two out-of-plane localized modes for which atoms move perpendicular to the surface; the modes have the frequencies  $\omega_d = 902.4$  and  $903.9$   $\text{cm}^{-1}$  ( $N_d = 99.55, 71.79$ ). See also the following animation files in the Supplemental Material:<sup>39</sup> I\_2\_902.gif through I\_2\_1749.gif.

An excess of two carbon atoms may lead to another concave deformation of the graphene lattice and two-adatom defect mode  $A_2(5556777)$  when, instead of six perfect hexagons, we have three pentagons, one hexagon, and three heptagons; see Fig. 4(b). Such a defect may appear when we remove four carbon atoms from the graphene lattice with Y-shape valent bonds, but instead insert six carbon atoms with a structure of a perfect hexagon. The transverse oscillations of this defect blister are considered in Ref. 40. As can be seen from Fig. 4,

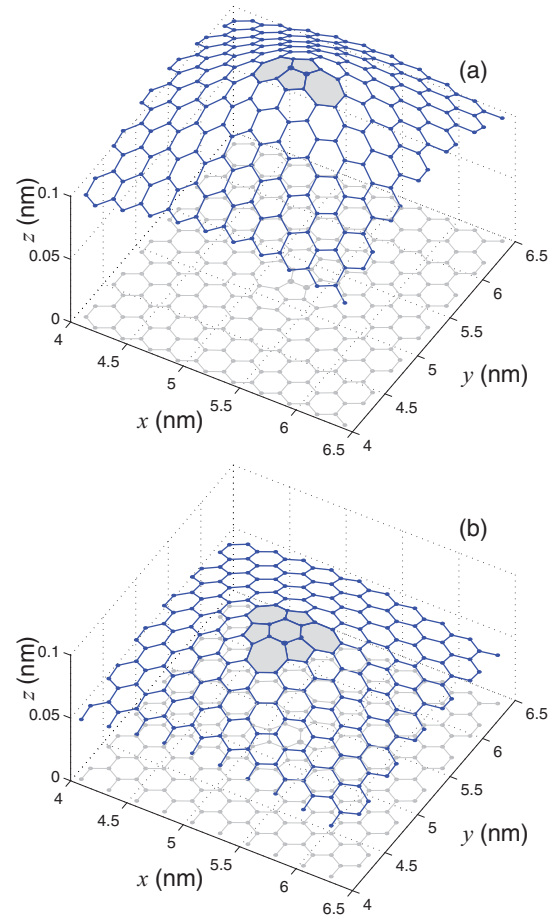


FIG. 4. (Color online) Deformation of the graphene sheet in the region of location of (a) inverse Stone-Wales defect  $I_2(7557)$  (two carbon adatoms with a valent bond are inserted in a perfect graphene lattice; they are shown by larger balls) and (b) two-adatom defect  $A_2(5556777)$ . The gray color is employed to show the change of the lattice structure introduced by the presence of a defect.

the defect  $I_2$  has a higher density of the atom localization in comparison with the defect  $A_2$  and, as a result, the defect  $I_2$  will bend the graphene sheet stronger than the defect  $A_2$ .

Our analysis of the localized oscillations of the graphene sheet demonstrates that the defect  $A_2(5556777)$  supports 11 localized modes for which the atoms move along a concave surface of the graphene sheet. The frequencies of those oscillations are  $\omega_d = 1601.0, 1603.3, 1604.2, 1608.6, 1610.7, 1613.6, 1614.6, 1617.8, 1682.4, 1704.2,$  and  $1706.4$   $\text{cm}^{-1}$  (participation numbers  $N_d = 131.01, 19.52, 22.49, 13.37, 7.28, 7.96, 19.94, 4.48, 3.94, 3.52, 2.77$ ). This defect supports also two out-of-plane oscillatory modes for which atoms move perpendicular to the graphene sheet; these modes have the frequencies  $\omega_d = 900.7$  and  $910.4$   $\text{cm}^{-1}$  ( $N_d = 85.54, 6.15$ ).

## VI. MODELING OF LOCALIZED OSCILLATIONS

To verify the results of our modal analysis, we model the oscillatory dynamics of a graphene with defects. We consider a graphene sheet of a finite extent, with the size of  $10.8 \times 10.6$   $\text{nm}^2$  and with a local defect at its center. To model the energy spreading in an effectively infinite graphene sheet, we

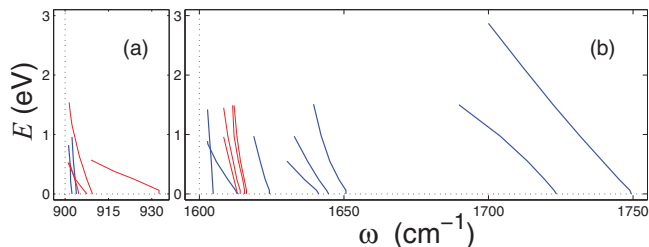


FIG. 5. (Color online) Dependencies of the energy  $E$  of localized defect modes vs frequency  $\omega$  for two types of defects: inverse Stone-Wales defect  $I_2(7557)$ , shown by blue (black) lines, and Stone-Wales defect  $SW(55-77)$ , shown by red (gray) lines. (a) and (b) show out-of-plane and in-plane oscillations, respectively. The vertical dotted line marks the edge of the linear spectrum band of phonons of the ideal graphene sheet.

introduce lossy boundary conditions, assuming that all edge atoms experience damping with relaxation time  $t_r = 10$  ps. If the excitation of the localized eigenmode leads to the creation of a localized state, or breathinglike mode, the kinetic energy will not vanish but instead will approach a certain nonzero value. Otherwise, the initial excitation will vanish completely, so that the kinetic energy

$$E_k = \sum_{n=1}^N \frac{1}{2} M(\dot{\mathbf{u}}_n, \dot{\mathbf{u}}_n)$$

will vanish when  $t \rightarrow \infty$ .

Our numerical simulation results demonstrate that all localized modes with the frequencies located outside the linear frequency bands of the ideal graphene sheet are stable. For small amplitudes, when the energy of the eigenmode is less than 0.06 eV, the amplitude and frequency of the mode do not change, which indicates that in that limit the oscillations are described by a linear theory. However, when more energy is pumped into the mode, we observe nonlinear effects when the frequency decreases with the energy, as shown in Fig. 5. In that case, the energy of the defect mode may exceed 1 eV.

We notice that the diagonalization of the matrix of the second derivatives,  $\mathbf{B} = (B_{jn})_{j,n=1}^N$ , also can give localized modes with the frequencies within the frequency bands of the ideal graphene sheet. However, numerical simulations demonstrate that such modes are not stable and the amplitude decays very rapidly.

## VII. INFLUENCE OF DEFECTS ON THE GRAPHENE'S FREQUENCY SPECTRA

Our results summarized above suggest that all frequencies of localized defect modes are located outside the linear bands of the oscillation spectrum of an ideal graphene sheet. This result is expected because any oscillation from the continuous spectrum is not spatially localized, and it corresponds to one of the extended modes. The splitting of the continuous modes of a perfect sheet of graphene and localized modes of the graphene with defects can be employed as an important fingerprint of the quality of the graphene honeycomb lattice. We demonstrate this approach for the case of a graphene sheet of a finite extent of  $3.93 \times 3.83$  nm<sup>2</sup> with inverse Stone-Wales defect  $I_2$ . This

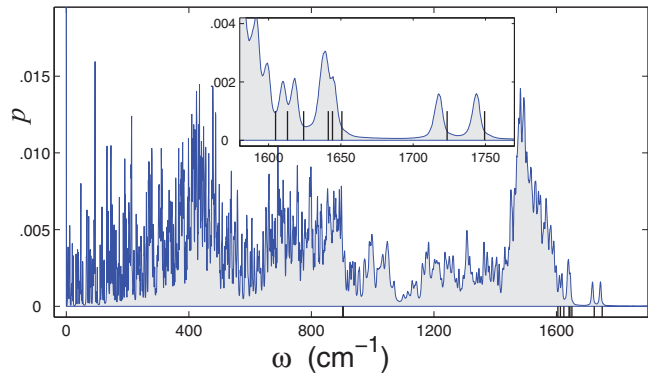


FIG. 6. (Color online) Frequency spectral density of thermal oscillations of a graphene sheet with inverse Stone-Wales defect  $I_2$  when two adatoms are inserted into the honeycomb lattice. The graphene sample consists of  $N = 578$  atoms and has the size of  $3.93 \times 3.83$  nm<sup>2</sup>, being placed at a temperature of  $T = 300$  K. The vertical solid bars show the frequencies of the localized oscillation of the defect modes.

patch of graphene has 578 carbon atoms, two of which create one pointlike defect of the type shown in Fig. 4(a).

In order to find the frequency spectrum of thermal oscillations of a graphene sheet, we place it in a Langevin thermostat at temperature  $T = 300$  K. After complete thermalization, we disconnect the graphene from the thermostat and study the oscillation spectra of the excited thermal oscillations.

The frequency spectral density of thermal oscillations of a sheet of graphene is shown in Fig. 6. As follows from those results, several additional peaks appear in the frequency spectrum above the upper edge of the spectral band of linear oscillations of a perfect graphene sheet ( $\omega > 1600$  cm<sup>-1</sup>). These peaks correspond to the eigenmodes of the localized oscillations of the defect  $I_2$ . Thus, from the specific structure of the frequency spectral density, we may judge about the types and density of structural defects in a particular graphene sample.

We notice that for a graphene flake placed on a substrate, the main results of our study will remain the same provided graphene does not create additional valent bonds with the substrate atoms. In this case, the interaction will shift the values of the frequencies of the localized defect modes by a few reversed centimeters. However, if the interaction of the graphene layer with the substrate creates new valent bonds, then the entire dynamics may change substantially, including the shape and oscillation frequencies of the defect modes.

## VIII. PHONON CONDUCTIVITY OF ARRAYS OF DEFECTS

The study of arrays of defects in graphene has attracted a lot of attention during recent years. It was shown that arrays of defects create a novel conduction pathway, which may serve as quantum wires in nanoscale electric network.<sup>14,15,18-21</sup> In all of those studies, the array is considered to be composed of a series of inverse Stone-Wales defects  $I_2(7557)$ , which can be realized experimentally in a graphene nanoribbon.<sup>41</sup>

Following those papers, we study the oscillatory dynamics of a zigzag nanoribbon with an array of inverse Stone-Wales

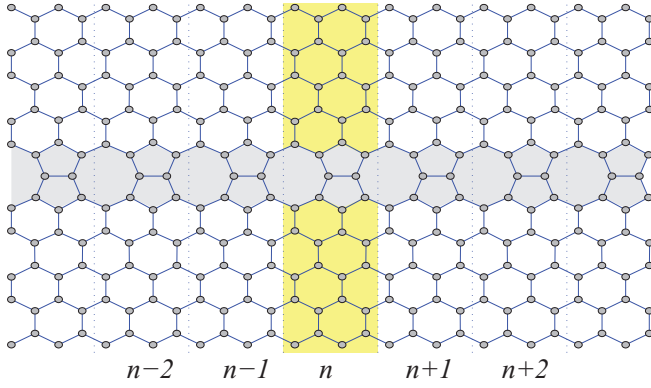


FIG. 7. (Color online) Schematic view of a zigzag nanoribbon with a straight chain of inverse Stone-Wales defects. The gray color is employed to show a change of the lattice structure introduced by the presence of defects. The yellow color marks one elementary cell of the nanoribbon with the dotted lines separating the elementary cells;  $n$  is the index of the elementary cell.

defects placed in its center, as shown in Fig. 7. If an ideal zigzag nanoribbon has  $K$  carbon atoms in its elementary cell, then the nanoribbon with the array of defects will have  $2(K + 1)$  carbon atoms in the elementary cell.

To describe nanoribbon oscillations, we write the system Hamiltonian in the form

$$H = \sum_n \left\{ \frac{1}{2} (\mathbf{M} \dot{\mathbf{x}}_n, \dot{\mathbf{x}}_n) + \mathcal{P}(\mathbf{x}_n, \mathbf{x}_{n+1}) \right\}, \quad (8)$$

where  $\mathbf{M}$  is the diagonal matrix of masses of all atoms of the elementary cell, and the  $\mathbf{x}_n - 6(K + 1)$ -dimensional vector describes the displacements of atoms from their equilibrium positions in the  $n$ th elementary cell.

Hamiltonian (8) generates the following set of the equations of motion:

$$-\mathbf{M} \ddot{\mathbf{x}}_n = \mathcal{P}_{\mathbf{x}_1}(\mathbf{x}_n, \mathbf{x}_{n+1}) + \mathcal{P}_{\mathbf{x}_2}(\mathbf{x}_{n-1}, \mathbf{x}_n). \quad (9)$$

In the linear approximation, this system takes the form

$$-\mathbf{M} \ddot{\mathbf{x}}_n = \mathbf{B}_1 \mathbf{x}_n + \mathbf{B}_2 \mathbf{x}_{n+1} + \mathbf{B}_2^* \mathbf{x}_{n-1}, \quad (10)$$

where the matrix elements are defined as

$$\mathbf{B}_1 = \mathcal{P}_{\mathbf{x}_1, \mathbf{x}_1} + \mathcal{P}_{\mathbf{x}_2, \mathbf{x}_2}, \quad \mathbf{B}_2 = \mathcal{P}_{\mathbf{x}_1, \mathbf{x}_2},$$

and the matrix of the partial derivatives takes the form

$$\mathcal{P}_{\mathbf{x}_i, \mathbf{x}_j} = \frac{\partial^2 \mathcal{P}}{\partial \mathbf{x}_i \partial \mathbf{x}_j}(\mathbf{0}, \mathbf{0}, \mathbf{0}), \quad i, j = 1, 2.$$

Solutions of the system of linear Eq. (10) can be sought in the standard form

$$\mathbf{x}_n = \mathbf{A} \mathbf{e} \exp(iqn - i\omega t), \quad (11)$$

where  $A$  is the mode amplitude,  $\mathbf{e}$  is the normalized dimensionless vector  $[(\mathbf{M} \mathbf{e}, \mathbf{e}) = 1]$ ,  $q \in [0, \pi]$  is the dimensionless wave number, and  $\omega$  is the phonon frequency. By substituting expression (11) into the system [Eq. (10)], we obtain the eigenvalue problem

$$\omega^2 \mathbf{M} \mathbf{e} = [\mathbf{B}_1 + \mathbf{B}_2 e^{iq} + \mathbf{B}_2^* e^{-iq}] \mathbf{e}. \quad (12)$$

Therefore, in order to find the dispersion relations characterizing the modes of the nanoribbon for each fixed value of the wave number  $0 \leq q \leq \pi$ , we need to find the eigenvalues of the Hermitian matrix [Eq. (12)] of the order  $6(K + 1) \times 6(K + 1)$ . As a result, the dispersion curves are composed of  $6(K + 1)$  branches,  $\{\omega_j(q)\}_{j=1}^{6(K+1)}$ . Two-thirds of the branches correspond to the atom vibrations in the plane of the nanoribbon  $xy$  (in-plane vibrations), whereas only one-third correspond to the vibrations orthogonal to the plane (out-of-plane vibrations), when the atoms are shifted along the  $z$  axes.

For deriving the modes localized on the array of defect, we select, from all dispersion curves, only the branches corresponding to the oscillation localized near the line of defects. To avoid the influence of edges, we consider an array with the width  $h = 25.5$  nm ( $K = 240$ ; the elementary cell consists of 482 atoms).

We assume that the nanoribbon oscillations are localized near the line of defects, provided 99% of its energy is concentrated in the center of the nanoribbon of the width  $h/2$ . The results of our analysis of these oscillations are summarized in Fig. 8. We observe that the array supports three types of oscillations described by three dispersion curves  $\omega(q)$ ,  $0 \leq q \leq \pi$ . Two branches describe out-of-plane oscillations, which appear above the frequency of out-of-plane vibrations

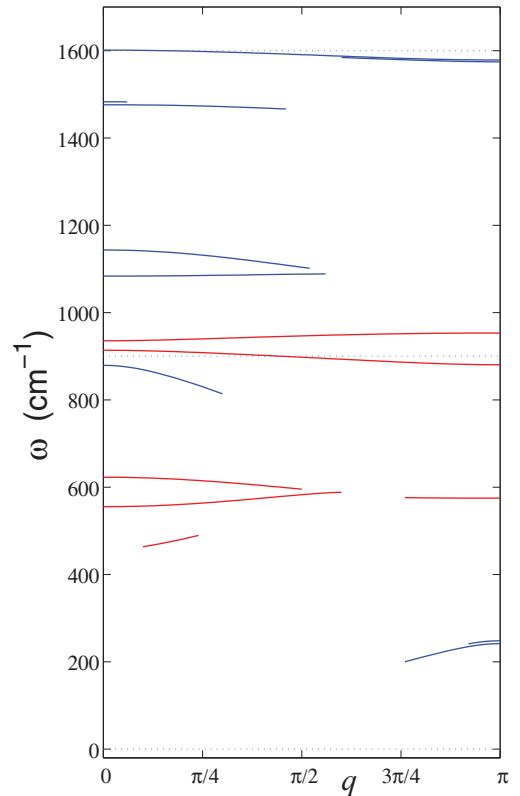


FIG. 8. (Color online) Dispersion curves of phonons localized on a chain of inverse Stone-Wales defects. Blue (black) curves correspond to in-plane vibrations; red (gray) curves correspond to the out-of-plane vibrations. The dotted lines mark the upper boundaries of the frequency spectrum ( $900 \text{ cm}^{-1}$ ) and in-plane small-amplitude oscillations of a planar sheet of graphene ( $1600 \text{ cm}^{-1}$ ), respectively.

of an ideal nanoribbon, and one branch describes in-plane vibrations with the frequency about the edge of the frequency spectrum of an ideal nanoribbon. In addition to the three complete branches, there are a few incomplete branches of the dispersion curves which are located inside the frequency spectrum of an ideal graphene nanoribbon.

Thus, the study of the spectrum of an array of defects demonstrates the appearance of minibands in the spectrum corresponding to the modes guiding along the array. It suggests that the array creates an effective one-dimensional waveguide for high-frequency phonons.

## IX. CONCLUSIONS

We have studied the effect of localized structural defects on the vibrational spectra of the graphene's oscillations. We have demonstrated that the local defects (such as Stone-Wales defects, one- and two-atom vacancies, many-atom linear vacancies, and adatoms) are characterized by stable localized oscillations with the frequencies lying outside the

linear frequency bands of the ideal graphene. In the frequency spectral density of thermal oscillations, such localized defect modes lead to the additional peaks located on the right side of the frequency band of the ideal sheet of graphene. Thus, the general structure of the frequency spectral density and its peaks can serve as a fingerprint of its quality and indicate both the type and quantity of the structural defects in a graphene sheet.

In addition, our analysis of localized eigenfrequency oscillatory modes of a wide graphene nanoribbon with an array of defects demonstrates that linear arrays of defects may play the role of efficient phononic waveguides that guide high-frequency phonons.

## ACKNOWLEDGMENTS

A.S. acknowledges the warm hospitality of the Nonlinear Physics Center at the Australian National University and thanks the Joint Supercomputer Center of the Russian Academy of Sciences for the use of their computer facilities. The work was supported by the Australian Research Council.

- 
- <sup>1</sup>H.-S. Philip Wong and Deji Akinwande, *Carbon Nanotube and Graphene Device Physics* (Cambridge University Press, Cambridge, 2011).
- <sup>2</sup>M. I. Katsnelson, *Graphene: Carbon in Two Dimensions*. (Cambridge University Press, Cambridge, 2012).
- <sup>3</sup>A. K. Geim and A. H. MacDonald, *Phys. Today* **60**, 35 (2007).
- <sup>4</sup>A. H. Castro Neto, F. Guinea, N. M. Peres, K. S. Novoselov, and A. K. Geim, *Rev. Mod. Phys.* **81**, 109 (2009).
- <sup>5</sup>Y.-H. Zhang, K.-G. Zhou, K.-F. Xie, X.-C. Gou, J. Zeng, H.-L. Zhang, and Y. Peng, *J. Nanosci. Nanotechnol.* **10**, 7347 (2010).
- <sup>6</sup>X. Qin, Q. Meng, Y. Feng, and Y. Gao, *Surf. Sci.* **607**, 153 (2013).
- <sup>7</sup>D. J. Appelhans, L. D. Carr, and M. T. Lusk, *New J. Phys.* **12**, 125006 (2010).
- <sup>8</sup>J. Song, H. Liu, H. Jiang, Q. F. Sun, and X. C. Xie, *Phys. Rev B* **86**, 085437 (2012).
- <sup>9</sup>F. Banhart, J. Kotakoski, and A. V. Krasheninnikov, *ACS Nano* **5**, 26 (2011).
- <sup>10</sup>N. Gorjizadeh, A. A. Farajian, and Y. Kawazoe, *Nanotechnology* **20**, 015201 (2009).
- <sup>11</sup>J.-H. Chen, W. G. Cullen, C. Jang, M. S. Fuhrer, and E. D. Williams, *Phys. Rev. Lett.* **102**, 236805 (2009).
- <sup>12</sup>J. Haskins, A. Kinaci, C. Sevik, H. Sevincli, G. Cuniberti, and T. Cagin, *ACS Nano* **5**, 3779 (2011).
- <sup>13</sup>F. Ding, K. Jiao, M. Wu, and B. I. Yakobson, *Phys. Rev. Lett.* **98**, 075503 (2007).
- <sup>14</sup>D. A. Bahamon, A. L. C. Pereira, and P. A. Schulz, *Phys. Rev. B* **83**, 155436 (2011).
- <sup>15</sup>L. Xiao-Ling, L. Zhe, Y. Hai-Bo, J. Li-Wei, G. Wen-Zhu, and Z. Yi-Song, *Phys. Rev. B* **86**, 045410 (2012).
- <sup>16</sup>A. Lherbier, Simon M.-M. Dubois, X. Declerck, Y.-M. Niquet, S. Roche, and J.-C. Charlier, *Phys. Rev. B* **86**, 075402 (2012).
- <sup>17</sup>X. Lin and J. Ni, *Phys. Rev. B* **84**, 075461 (2011).
- <sup>18</sup>M. Kan, J. Zhou, Q. Sun, Q. Wang, Y. Kawazoe, and P. Jena, *Phys. Rev. B* **85**, 155450 (2012).
- <sup>19</sup>M. Pelc, L. Chico, A. Ayuela, and W. Jaskolski, *Phys. Rev. B* **87**, 165427 (2013).
- <sup>20</sup>T. Hu, J. Zhou, J. Dong, and Y. Kawazoe, *Phys. Rev. B* **86**, 125420 (2012).
- <sup>21</sup>L. Jiang, G. Yu, W. Gao, Z. Liu, and Y. Zheng, *Phys. Rev. B* **86**, 165433 (2012).
- <sup>22</sup>H. Huang, Y. Xu, X. Zou, J. Wu, and W. Duan, *Phys. Rev. B* **87**, 205415 (2013).
- <sup>23</sup>D. Yang, F. Ma, Y. Sun, T. Hu, and Kewei Xu, *Appl. Surf. Sci.* **258**, 9926 (2012).
- <sup>24</sup>D. W. Noid, B. G. Sumpter, and B. Wunderlich, *Macromolecules* **24**, 4148 (1991).
- <sup>25</sup>B. G. Sumpter, D. W. Noid, G. L. Liang, and B. Wunderlich, *Adv. Polym. Sci.* **116**, 27 (1994).
- <sup>26</sup>A. V. Savin and L. I. Manevitch, *Phys. Rev. B* **58**, 11386 (1998).
- <sup>27</sup>A. V. Savin and L. I. Manevitch, *Phys. Rev. E* **61**, 7065 (2000).
- <sup>28</sup>A. V. Savin and L. I. Manevitch, *Phys. Rev. B* **67**, 144302 (2003).
- <sup>29</sup>A. V. Savin and Yu. S. Kivshar, *Europhys. Lett.* **82**, 66002 (2008).
- <sup>30</sup>D. Gunlycke, H. M. Lawler, and C. T. White, *Phys. Rev. B* **77**, 014303 (2008).
- <sup>31</sup>A. V. Savin, Yu. S. Kivshar, and B. Hu, *Phys. Rev. B* **82**, 195422 (2010).
- <sup>32</sup>A. V. Savin, Yu. S. Kivshar, and B. Hu, *Europhys. Lett.* **88**, 26004 (2009).
- <sup>33</sup>A. V. Savin, B. Hu, and Yu. S. Kivshar, *Phys. Rev. B* **80**, 195423 (2009).
- <sup>34</sup>A. V. Savin and Yu. S. Kivshar, *Appl. Phys. Lett.* **94**, 111903 (2009).
- <sup>35</sup>A. V. Savin and Yu. S. Kivshar, *Europhys. Lett.* **89**, 46001 (2010).
- <sup>36</sup>A. V. Savin and Yu. S. Kivshar, *Phys. Rev. B* **81**, 165418 (2010).
- <sup>37</sup>D. W. Brenner, O. A. Shenderova, J. A. Harrison, S. J. Stuart, B. Ni, and S. B. Sinnott, *J. Phys.: Condens. Matter* **14**, 783 (2002).
- <sup>38</sup>A. V. Savin and Yu. S. Kivshar, *Phys. Rev. B* **85**, 125427 (2012).
- <sup>39</sup>See Supplemental Material at <http://link.aps.org/supplemental/10.1103/PhysRevB.88.125417> for movies that show the oscillatory dynamics off localized modes.
- <sup>40</sup>C.-W. Pao, T.-H. Liu, C.-C. Chang, and D. J. Srolovitz, *Carbon* **50**, 2870 (2012).
- <sup>41</sup>J. Lahiri, Y. Lin, P. Bozkurt, I. I. Oleynik, and M. Batzill, *Nat. Nanotechnol.* **5**, 326 (2010).